Crystal structure of (La,Ca)MnO₃ ultrathin films deposited on SrTiO₃ substrates

Y. L. Qin , H. W. Zandbergen , Z. Q. Yang & J. Aarts

Full Terms & Conditions of access and use can be found at
http://www.tandfonline.com/action/journalInformation?journalCode=tphm20

Crystal structure of (La,Ca)MnO$_3$ ultrathin films deposited on SrTiO$_3$ substrates

Y. L. QIN*†, H. W. ZANDBERGEN†, Z. Q. YANG‡ and J. AARTS‡

†National Centre for High-resolution Electron Microscopy,
Laboratory of Materials Science, Delft University of Technology,
Rotterdamseweg 137, 2628 AL Delft, The Netherlands
‡Kamerlingh Onnes Laboratory, Leiden University, P.O. Box 9504,
2300 RA Leiden, The Netherlands

Epitaxial La$_{1-x}$Ca$_x$MnO$_3$ ($x \cong 0.33$) ultrathin films with thickness between 3 and 6 nm have been grown on (001) SrTiO$_3$ substrates by sputter deposition. The films do not exhibit an insulator-metal transition as a function of temperature, which is normal in thicker films. High-resolution transmission electron microscopy and electron diffraction were used to investigate the crystal structure. It was found that the films grow coherently on the substrates and are perfectly crystalline. Their crystal structure was determined to be a body-centred orthorhombic structure with space group *Imma*, instead of the orthorhombic *Pnma* bulk structure. This structure change is probably responsible for the insulating property of the films.

1. Introduction

Thin films of perovskite manganite Ln$_{1-x}$A$_x$MnO$_3$ (where Ln is a lanthanide, and A is a divalent alkalai dopant) have attracted considerable attention over the last decade, because they exhibit a variety of interesting properties, such as colossal magnetoresistance, which is potentially useful in magnetic sensors and information recording device applications [1–3]. One fascinating issue that has been subjected to investigation is substrate-induced strain effects in epitaxial thin films grown onto various substrates. Thin manganite films display properties different from those of bulk materials, and several groups have reported interesting properties such as anisotropic magnetoresistance (MR) [4–6], magnetic anisotropies [7, 8] and magnetic domain structures [9] in manganite thin films. Recently, Wang *et al.* [10] reported a study of structural and magnetotransport properties of Pr$_{0.67}$Sr$_{0.33}$MnO$_3$ films with thickness in the range 4–400 nm. It was found that the metal-insulator (MI) transition temperatures, T_p, and MR properties depend strongly on the film thickness, t, in the strained samples. When t is less than 20 nm, T_p drops sharply with decreasing t accompanied by a sharp increase of high-field MR. An earlier study

---

*Corresponding author. Email: yqin2@andrew.cmu.edu; y.qin@rug.nl

on $La_{0.67}Sr_{0.33}MnO_3$ thin films also showed a fast increase in resistivity upon thickness reduction, and the MI transition was depressed in the thinnest film grown on $LaAlO_3$ substrates [11]. The authors attributed these to a chemically or structurally altered surface and/or interface dead layer, which is about 3–5 nm thick depending on the substrate. However, the crystal structure of this dead layer has not been well studied.

So far, there have been few reports on the crystal structure of the manganite thin films, which are most commonly described as tetragonally distorted perovskite [4–11]. Lebedev *et al.* [12] have studied the structure of (La,Ca)MnO$_3$ (LCMO) thin films, deposited on $SrTiO_3$ (STO) substrates. The structure of the LCMO thin films with a thickness of 250 nm was found to alter from the bulk orthorhombic *Pnma* structure to a monoclinic *P2$_1$/c*. For thin (<20 nm) LCMO films on STO, Zandbergen *et al.* [13, 14] have shown that the structure remained orthorhombic but with a loss of the octahedral tilting about the *b* axis that is normal for the bulk *Pnma* structure.

In our present work, we studied the strain effects in $La_{1-x}Ca_xMnO_3$ ($x \cong 0.33$) thin films grown on STO substrates. Films with larger thickness (6–200 nm) show the usual MI transition as a function of temperature, but for thicknesses below 6 nm the films became increasingly insulating, leading to a ferromagnetic insulating ground state but still with a large MR ratio in high magnetic fields. The details of the physical properties studied have been published elsewhere [15]. In this paper, high-resolution transmission electron microscopy (HRTEM) imaging and electron diffraction (ED) are used to investigate the crystal structure of LCMO ultrathin films with thicknesses less than 6 nm. These films are found to be insulating in the whole temperature range, and their structure was determined to be body-centred orthorhombic (bco) with a space group of *Imma*. In the previous report [15], we determined the crystal structure to be body-centred tetragonal (bct) with space group *I4/mcm*. That structure very closely resembles the *Imma* structure, but the more refined analysis presented here leads to the conclusion of the structure being bco, as will be discussed.

2. Experimental procedures

LCMO films with thickness in the range 3 to 6 nm were deposited on (001)-oriented single-crystal STO substrates by magnetron-sputter deposition with very low growth rates. Details of the growth procedure have been described elsewhere [15]. Cross-sectional specimens for TEM observations were prepared by ion milling. Firstly, the samples were cut onto slices along the [100] and [110] directions of STO. The slices were then glued with silicon and mechanically ground directly down to a homogeneous thickness less than 10 μm. During ion milling, the specimens were not rotated and oriented such that the thin-film side was facing away from ion gun. HRTEM and ED were performed with a Philips CM 30UT electron microscope with a field-emission gun operated at 300 kV. A condenser aperture of 10 μm and a small spot size of 5 nm were used to obtain ED patterns from the ultrathin films. The image simulations of proposed structure model were carried out with Mac Tempas software. For the basic structure simulation, different specimen thickness in the

range 5 to 9.5 nm and defocus values in the range from -5 to -20 nm were used. The calculated images were compared with the observed HRTEM images.

3. Results

An important feature of the structure of LCMO is the tiltings of the MnO$_6$ octahedra. For bulk samples of LCMO, with $x = 0.30$–0.33, it leads to an orthorhombic structure with space-group *Pnma* and axes being approximately $a = 2^{1/2}a_p$, $b = 2a_p$, $c = 2^{1/2}a_p$, where a_p is the simple perovskite cubic lattice parameter [16, 17]. The superstructure is strongly correlated to the tilts of the octahedra. STO has a simple cubic structure without any tilts. To specify the directions in this paper we will use the substrate directions. In order to distinguish the directions of different phases a subscript will be added to the directions and planes of the specified phase, e.g. [100]$_{STO}$ for [100] orientation of STO, and [010]$_{Pnma}$ for [010] orientation of the *Pnma* structure of the LCMO films.

3.1. *High-resolution images*

Figure 1a shows an HRTEM image of a LCMO thin film (about 3 nm) viewed parallel to the interface along the [100]$_{STO}$ orientation. The HRTEM image of the interface shows that the LCMO film is perfectly coherent across the interface, which is completely free of any defects. One surprising feature of this image is that no evidence is found for the image contrast expected for the bulk orthorhombic *Pnma* unit cell. Such a unit cell usually produces (010)$_{Pnma}$ $2a_p$ double fringes in images taken parallel to [101]$_{Pnma}$ or [10$\bar{1}$]$_{Pnma}$, or a $2^{1/2}a_p$ (100)$_{Pnma}$ and (001)$_{Pnma}$ fringes in the [010]$_{Pnma}$ image. Although this $2a_p$ fringe cannot be observed for the perfect [101]$_{Pnma}$ or [10$\bar{1}$]$_{Pnma}$ orientation of space group *Pnma*, Zandbergen and Jansen [18] have shown that it can be obtained by symmetry-breaking either at the crystal (by a misorientation) or in the imaging (by beam tilt or astigmatism). These (010)$_{Pnma}$ fringes are observed in our thicker films (>6 nm) and are systematically absent in the ultrathin films (<6 nm). The absence of the superstructure fringes in HRTEM images or superlattice spots in the ED pattern indicates that the crystal structure is not the *Pnma* orthorhombic. Since on the other hand super-reflections are visible along other viewing directions, the structure still deviates from STO. A first consideration of these super-reflections suggests a cubic structure with either a primitive unit cell or a face-centred cubic (fcc) unit cell with $a_{fcc} \approx 2a_p$. Figures 1b and 1c show the HRTEM images of the same 3 nm LCMO film viewed along [1$\bar{1}$0]$_{STO}$ and [110]$_{STO}$ directions, respectively. They exhibit two different easily recognizable high-resolution image patterns. Figure 1b shows a simple cubic pattern, whereas figure 1c shows a superstructure and body-centered rectangular symmetry.

3.2. *Electron diffraction patterns*

The HRTEM images shown in figure 1 indicate that the crystal structure of the 3-nm LCMO films deviates from *Pnma* symmetry. In order to study the structure of the 3-nm films, we performed a systematic electron diffraction study. Figure 2 shows five ED patterns obtained by focusing the electron beam to a diameter of about 5 nm
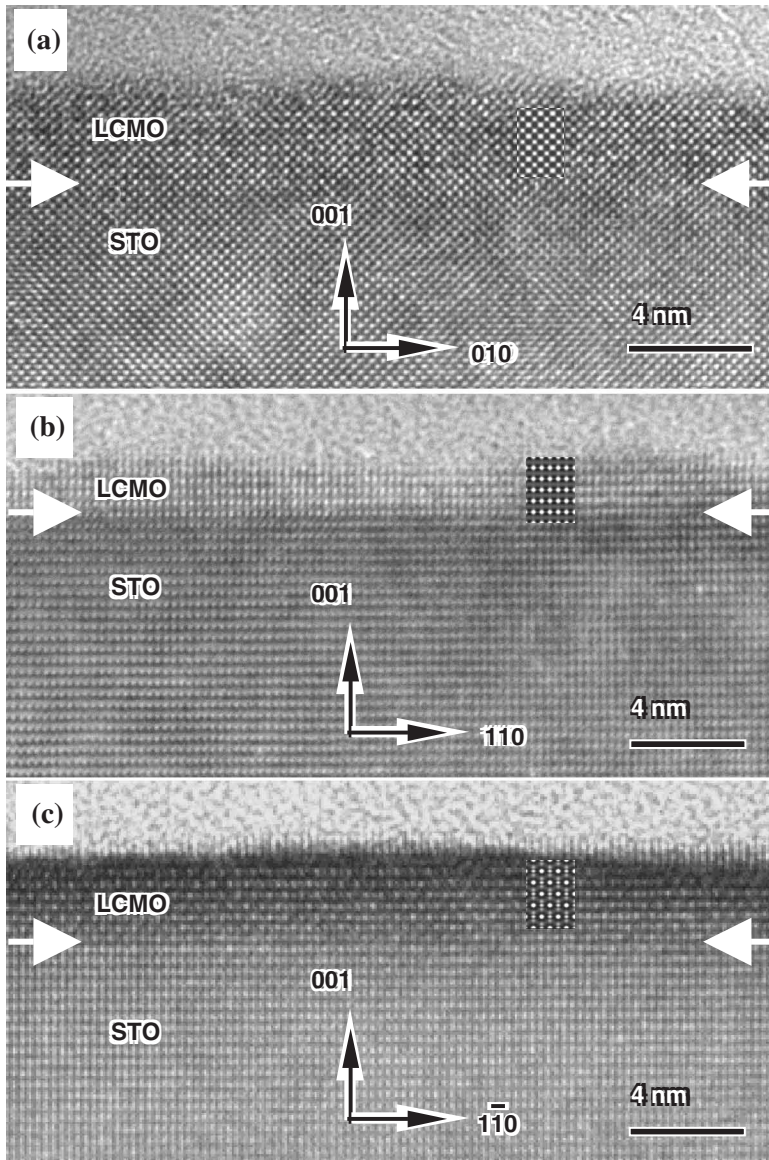
Figure 1. Cross-sectional HRTEM images of a 3 nm LCMO ultrathin film taken along (a) $[100]_{STO}$, (b) $[1\bar{1}0]_{STO}$ and (c) $[110]_{STO}$ directions, respectively. Note the superstructure pattern in (c) is not presented in (b). The calculated images are given as insets: thickness $t = 8$ nm and defocus value $\Delta f = -45$ nm for (a), and -15 nm for (b) and (c).

and including both film and substrate. Figure 2a was obtained from the $[100]_{STO}$ direction; no super-reflections can be observed, which is in consistent with the HRTEM image (figure 1a). In contrast with figure 2a super-reflections were found in other directions. By tilting the sample along the $[001]_{STO}$ axis, two patterns containing super-reflections ($[510]_{STO}$ (figure 2b) and $[310]_{STO}$ (figure 2c))
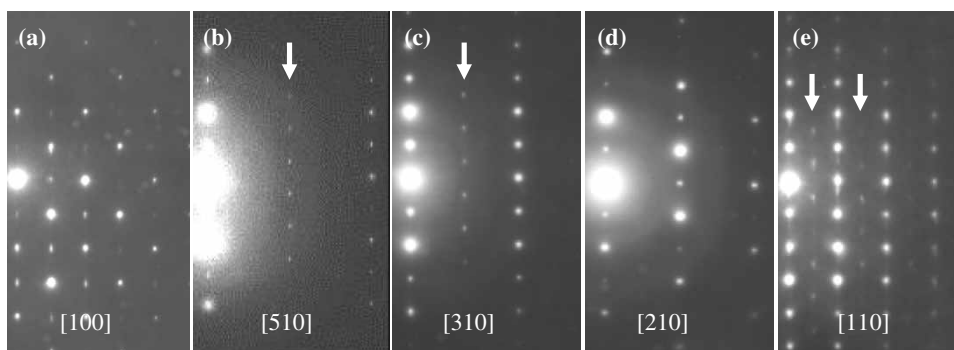
Figure 2. Electron diffraction patterns of the 3 nm LCMO ultrathin film (obtained by tilting the sample along the $[001]_{STO}$ axis) which has been indexed as a simple-cubic structure. Note the presence of super-reflections as marked by arrows in (b), (c) and (e).

were obtained. In figures 2b and 2c, the distance between the spots in the extra row of spots (marked by arrows) corresponds to the c_{STO} axis. In addition, the spots are shifted by a distance of one-half spacing, relative to the spot positions of the neighbouring lines. Reconstruction of these five ED patterns suggests a body-centred cubic lattice structure in reciprocal space, corresponding approximately to a face-centred pseudo-cubic lattice in real space with a unit cell of $2a_p \times 2a_p \times 2a_p$. It is noteworthy that this pseudo fcc structure has also been reported in as-grown LCMO films on $LaAlO_3$ substrates [19].

The basic perovskite structure of bulk LCMO has a lattice parameter of $a_p = 0.387$ nm, which is smaller than that of STO ($a_{STO} = 0.3905$ nm) at room temperature. Hence, the LCMO films are expanded biaxially in the film plane. Correspondingly, the in-plane lattice parameter is lattice matched to that of the 0.3905 nm lattice constant of STO substrate since there are no misfit dislocations at the interface, and consequently the out of plane axis is expected to compress according to the Poisson ratio, resulting in a tetragonal distortion. This tetragonal distortion has been reported by many authors in various manganite films grown on different substrates [4–11]. Because of the very thin film thickness as well as the relaxation in the HRTEM specimen due to the small thickness of the cross-section specimen [18], this tetragonal distortion cannot be measured precisely on the HRTEM images and ED patterns. Our previous X-ray diffraction experiments on the thicker films do reveal this tetragonal distortion. Films grown on STO up to 200 nm have a slightly thickness-dependent out of plane parameter [20]. Extrapolated to the 3 nm films, an out of plane parameter of 0.382 nm would be obtained. However, recently de Andrés *et al.* [21] studied the crystal structure of LCMO films with thicknesses ranging from 2.4 to 80 nm by X-ray diffraction. The diffractometer at the DUBBLE-BM26 beamline at the Europen Synchronton Radiation Facility allowed these authors to obtain the diffraction patterns from the thinnest 2.4-nm films. The films that were thicker than 6.6 nm show a similar *Pnma* orthorhombic structure, whereas the 2.4-nm film adopts a different structure. The extinction conditions of the 2.4-nm film can also be attributed to the face-centred pseudo-cubic structure. For example, only integer peaks in the $(1, 0, l)$
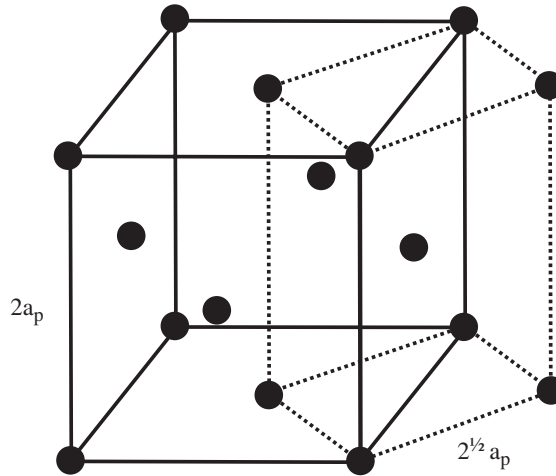
Figure 3. A schematic of the relationship between a face-centred cubic $2a_p \times 2a_p \times 2a_p$ cell (outlined by the solid line) and a body-centred tetragonal or orthorhombic $2^{1/2}a_p \times 2^{1/2}a_p \times 2a_p$ cell (outlined by the dashed line).

scan and half-integer peaks in the $(1.5, 0.5, l)$ scan appeared for the 2.4-nm film. According to de Andrés *et al.* [21], the 2.4-nm film follows the STO parameter in the film plane, while the out of plane parameter is slightly reduced. Remarkable is that the 2.4-nm film shows a slightly larger out of plane parameter than that of the thicker films, probably due to the structural phase transition. In this paper, we will adopt the unit-cell parameters from de Andrés *et al.* [21], $a = 0.3905$ nm and $c = 0.387$ nm, leading to an axis ratio $c/a = 0.991$, where a and c are the in plane and out of plane parameters of the simple perovskite, respectively. Because of this tetragonal distortion, the $2a_p \times 2a_p \times 2a_p$ fcc structure is actually a bct or bco structure with a unit cell of $\sim 2^{1/2}a \times 2^{1/2}a \times 2c$. The relationship between the fcc and bct/bco lattice cells is shown in figure 3.

3.3. *Space group determination*

It is well known that the perovskite structure is very prone to subtle structural transformations due to lattice distortions, which can be attributed to distortions or/and tilting of the octahedra. Various perovskite structures can be derived from the 23 Glazer tilt systems [22]. For example, the bulk structure *Pnma* can be obtained from the tilt systems $a^+b^-b^-$ or $a^+a^-a^-$. In thin films deviations from the cubic structure can become more pronounced owing to the influence of the substrates, especially at very thin thickness. Following Woodward [23], the space group and unit cell associated with each tilting system can be deduced. Considering the fourfold symmetry of the $(001)_{STO}$ plane of the STO substrate and the thickness of the films, the most likely tilting system would be a one-tilt or a two-tilt system, whose space group and unit cell are listed in table 1. It is very clear that only two tilting systems, i.e. $a^0a^0c^-$ and $a^0b^-b^-$ give a body-centred structure with unit cell of $\sim 2^{1/2}a_p \times 2^{1/2}a_p \times 2a_p$. Therefore, the 3-nm films in our study and probably also

Table 1. Space groups and their unit cells for the one-tilt and two-tilt systems. The three-tilt systems resulting in the LCMO bulk structure *Pnma* are also listed for comparison. The number in the first column is the tilt system number according to Woodward [23]. The number in the second column is the space group number in International Table for crystallography [24].

| Tilt system symbol	Space group	Bravais lattice	Unit cell size
$a^+b^-b^-$ (10)	*Pnma* (#62)	Primitive orthorhombic	$\sim 2^{1/2}a_p \times 2a_p \times 2^{1/2}a_p$
$a^+a^-a^-$ (11)			
$a^0b^+c^+$ (15)	*Immm* (#71)	Body-centred orthorhombic	$\sim 2a_p \times 2a_p \times 2a_p$
$a^0b^+b^+$ (16)	*I4/mmm* (#139)	Body-centred tetragonal	$\sim 2a_p \times 2a_p \times 2a_p$
$a^0b^+c^-$ (17)	*Cmcm* (#63)	C-centred orthorhombic	$\sim 2a_p \times 2a_p \times 2a_p$
$a^0b^+b^-$ (18)			
$a^0b^-c^-$ (19)	*I2/m* (#12-3)	Monoclinic	$\sim 2^{1/2}a_p \times 2a_p \times 2^{1/2}a_p$; $\beta \neq 90°$
$a^0b^-b^-$ (20)	*Imma* (#74)	Body-centred orthorhombic	$\sim 2a_p \times 2^{1/2}a_p \times 2^{1/2}a_p$
$a^0a^0c^+$ (21)	*P4/mbm* (#127)	Primitive tetragonal	$\sim 2^{1/2}a_p \times 2^{1/2}a_p \times 2a_p$
$a^0a^0c^-$ (22)	*I4/mcm* (#140)	Body-centred tetragonal	$\sim 2^{1/2}a_p \times 2^{1/2}a_p \times 2a_p$
$a^0a^0a^0$ (23)	*Pm$\bar{3}$m* (#221)	Primitive cubic	$\sim a_p \times a_p \times a_p$
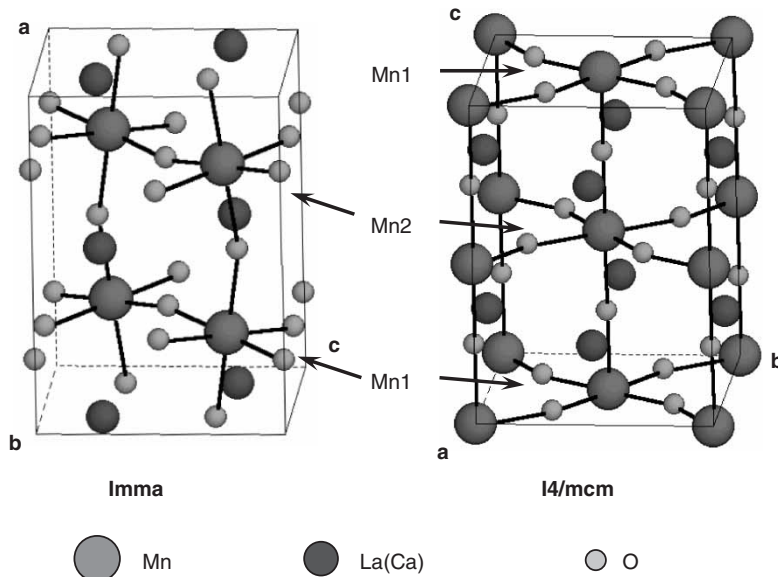
Figure 4. Comparison of proposed unit cell of (La,Ca)MnO₃ based on two space groups *Imma* and *I4/mcm*. The MnO₂ layers are marked by arrows.

the 2.4-nm film of de Andrés *et al.* [21] have either a bct *I4/mcm* structure or a bco *Imma* structure. The tetragonal *I4/mcm* structure is a result of rotation of the MnO_6 octahedra around the out of plane axis, while the orthorhombic *Imma* structure arises from the rotations of the MnO_6 octahedra around the two perovskite cubic axes in the film plane. Structural models based on *Imma* and *I4/mcm* are shown in figure 4. In *Imma* all MnO_6 octahedra remain essentially undeformed and the tilts

are coupled. In *I4/mcm* on the other hand, MnO_6 octahedra are deformed in order to keep the axes ratio $c/a < 1$.

In order to determine the actual structure in the LCMO ultrathin films, the diffraction conditions are firstly examined. With reference to the orthorhombic *Imma* description, all diffraction conditions are found to be satisfied: *hkl*: $h+k+l=2n$; *0kl*: $k+l=2n$; *h0l*: $h+l=2n$; *hk0*: $h=2n$ and $k=2n$; *h00*: $h=2n$; *0k0*: $k=2n$; *00l*: $l=2n$. As for the tetragonal *I4/mcm* description, all other diffraction conditions are also satisfied, except the reflections *0kl*: $k+l=2n$. This is not consistent with the diffraction conditions of the generally assumed *I4/mcm* space group since this would require *0kl*: $k=2n$ and $l=2n$.

The high-resolution images in figures 1b and 1c can be explained as being viewed along $[001]_{Imma}$ and $[010]_{Imma}$ axis zones of *Imma*, respectively. In the *Imma* space group-based structure, the successive layers of MnO_6 octahedra along $[100]_{Imma}$ have a different geometry in projection along viewing direction $[010]_{Imma}$ (figure 5a), but an identical geometry in projection along viewing
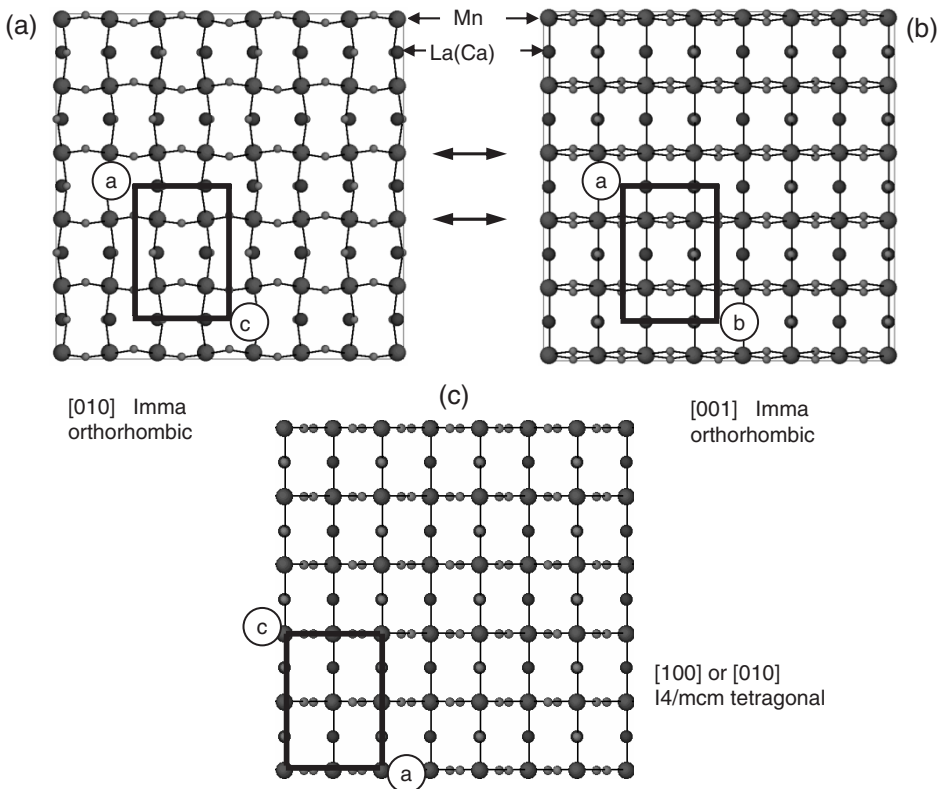

Figure 5.   Comparison of proposed structures of $(La,Ca)MnO_3$ based on two space groups. (a) $[010]_{Imma}$ orthorhombic and (b) $[001]_{Imma}$ zone view of the orthorhombic structure (*Imma*), and (c) $[100]_{I4/mcm}$ or $[010]_{I4/mcm}$ zone view of the tetragonal structure (*I4/mcm*). The unit cells are outlined by solid rectangles.

direction $[001]_{Imma}$ (figure 5b). However, they are identical in both projections along the $[100]_{I4/mcm}$ and $[010]_{I4/mcm}$ directions in the *I4/mcm*-based structure (figure 5c).

HRTEM image simulations have been performed based on the orthorhombic *Imma* structure. The fractional atomic coordinates are summarized in table 2. The cation atoms are kept fixed at the position of the ideal perovskite structure and the positions of O1 and O2 are selected so that all the MnO_6 octahedra are undistorted and tilted leading to a ratio of $c/a = 0.991$. The observed superstructure in $[010]_{Imma}$ image is apparent, as can be deduced from simulated images (figure 6a). It should be noted that the channels in the La(Ca)O layers are imaged as the brightest dots in the $[001]_{Imma}$ images. The superstructure in $[010]_{Imma}$ is due to the fact

Table 2. Positional parameters for $La_{0.7}Ca_{0.3}MnO_3$ (space group *Imma*), $a_{Imma} = 0.774$ nm, $b_{Imma} = 0.552$ nm, and $c_{Imma} = 0.552$ nm.

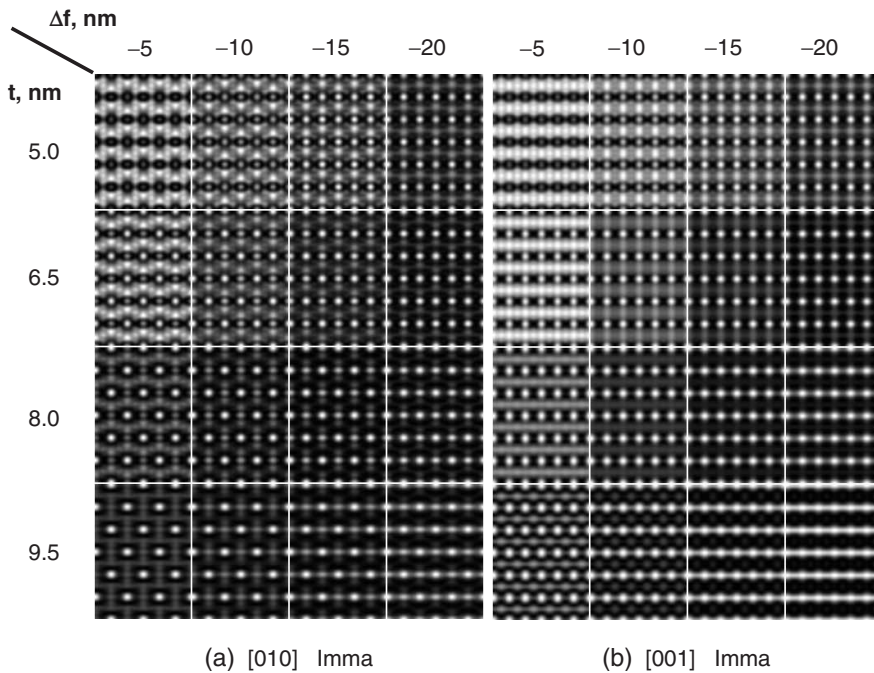| Atom	x	y	z	Occup.
La	0	0.25	0.75	0.7
Ca	0	0.25	0.75	0.3
Mn	0.25	0.25	0.25	1
O(1)	0	0.25	0.3	1
O(2)	0.22	0	0	1

Figure 6. Matrix of simulated images of the orthorhombic structure *Imma* along [010] (a) and [001] (b) zones. The specimen thickness was varied from 5.0 to 9.5 nm and the defocus was varied over the range of −5 to −20 nm in steps of −5 nm.

that neighbouring channels are imaged as dots with a different "grayness" or even disappear at specific imaging conditions. The simulated images, calculated for the orthorhombic cell *Imma*, are also superposed on the experimental images in figure 1.

4. Discussion

The structure of the LCMO system is complex owing to structural distortions that lead to a variety of closely related pseudocubic crystal structures. In the literature, a fcc pseudocubic with a double-perovskite unit cell $\sim 2a_p \times 2a_p \times 2a_p$ was usually reported [19]. However, this lattice structure could not be deduced from the 23 Glazer tilt systems, unless a $1:1$ Mn^{3+}/Mn^{4+} ordering occurs, which is not the case in our study. Owing to the mismatch of the substrate, the out of plane parameter of the ultrathin films is different from the in plane parameters, leading to a pseudo-tetragonal structure of parameters $\sim 2^{1/2}a_p \times 2^{1/2}a_p \times 2a_p$. The possible crystal structure would be a body-centred tetragonal *I4/mcm* or a body-centred orthorhombic *Imma* according to Woodward [23]. The tetragonal *I4/mcm* structure is a one-tilt system, while the orthorhormbic *Imma* structure is a two-tilt system. If all MnO_6 octahedra remain undeformed and the tilts are coupled, the *I4/mcm* structure would have a ratio of $c/a > 1$, whereas the *Imma* structure leads to a ratio of $c/a < 1$ (see figure 4). In the presently studied LCMO films, the larger lattice of the STO substrate leads to an expansion of the LCMO lattice to fit the substrate. The volume increase associated with this in-plane matching is partly compensated by a lattice contraction along the interface normal ($c/a < 1$). This would favour the formation of the *Imma* structure, because in the *I4/mcm* structure the tilt about the c axis leads to a decrease in the in-plane axes, whereas for the matching to the substrate a lattice expansion is required. Therefore, in the latter case a Jahn-Teller (JT) distortion of the octahedra would be required in order to provide a better lattice match with the larger STO substrate. This JT distortion will result in an elongation in the film plane in combination with a reduction in the c direction. On the other hand, if films are grown on a substrate with a smaller lattice, e.g. $LaAlO_3$, this JT distortion will be not necessary, and the LCMO films would adopt the *I4/mcm* structure. It is interesting to note that Wang *et al.* [10] have observed that the $Pr_{0.67}Sr_{0.33}MnO_3$ films under biaxial tensile-strain show different T_p from under compressive-strain.

Our previous studies [13, 14] indicated that LCMO films thicker than about 40 nm show domain structures, with the three possible directions of the b axis. In the LCMO films thinner than 40 nm, the b axis is always perpendicular to the interface. However, twin boundaries, due to an interchange of the a and c axes, were observed. The average spacing of such twin boundaries is reduced from about 30 nm to about 10 nm as the LCMO film thickness decreases from 12 to 6 nm. However, the present studied 3-nm LCMO films seem to have a single crystalline domain, or at least the domain size is larger than the observed area under TEM, i.e. ~ 500 nm. This is generally in accordance with the X-ray results of de Andrés *et al.* [21]: as the thickness of LCMO films is reduced, the *Pnma* structure is maintained by decreasing the domain size until a phase transition occurs, which allows a larger size of the in-plane structural domain.

The insulating property of the ultrathin films can be attributed to the fully strained bco *Imma* structure. All the LCMO films with a thickness of >6 nm, that show MI transition, always have the same *Pnma* orthorhombic structure as the bulk material. However, the films with smaller thickness, that do not exhibit a MI transition, always adopt the bco *Imma* structure. It seems that 6 nm is a critical thickness for the bco structure to be stable in the thin films; when the thickness is larger than 6 nm, films restore the bulk orthorhombic *Pnma* structure. This thickness is quite consistent with the dead layer observed in $La_{0.67}Sr_{0.33}MnO_3$ films [11], which is probably also related to this structure. The change of structure in the ultrathin films from an orthorhombic *Pnma* structure to a bco *Imma* structure would quite naturally have a large influence on many relevant properties. For example, the change of the tilts of the MnO_6 octahedra would affect the Mn–O bond length and Mn–O–Mn bond angle, thus influencing the magnetic or electronic exchange interactions between two magnetic cations separated by an anion. In the present studies, the thinnest 3-nm films show insulating behaviour without MR effects, while a slightly thicker 5-nm film showed MR effects but still no IM transition. HRTEM images and ED patterns (not shown) revealed that the 5-nm films have the same bco *Imma* structure. However, increasing the thickness leads to a gradual change to the bulk three-tilt *Pnma* structure. A mixture of the *Pnma* and the bco *Imma* structures was found in the 5-nm films. Figure 7 shows an ED pattern obtained
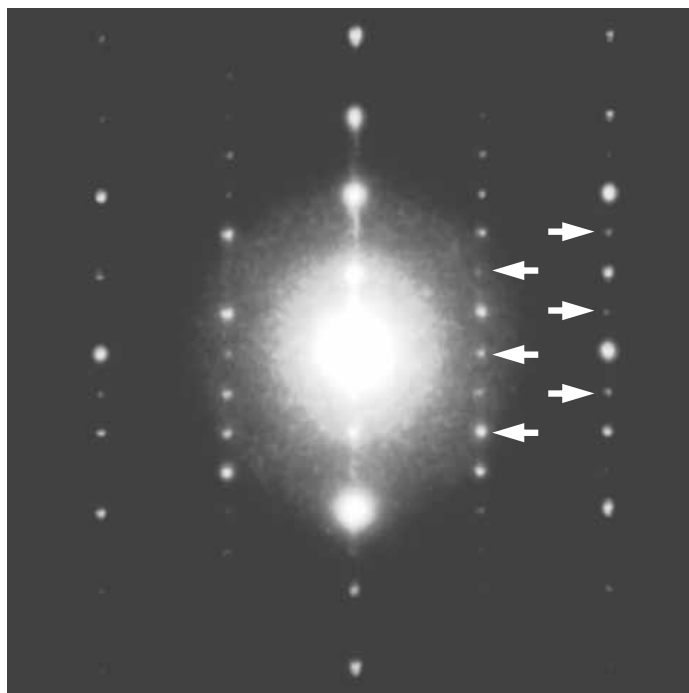

Figure 7. Electron diffraction pattern of a 5 nm LCMO film along $[310]_{STO}$ direction. Compared with figure 2(c) extra super-reflections present as marked by arrows, which indicate that it be indexed as the $[201]_{Pnma}$ zone pattern of the *Pnma* structure.

occasionally from the 5-nm LCMO films along the $[310]_{STO}$ direction, which can be indexed as $[201]_{Pnma}$ zone pattern of the *Pnma* structure.

5. Conclusions

In conclusion, we have studied the crystal structure of LCMO ultrathin films with thickness less than 6 nm. The LCMO ultrathin films were found to grow coherently on STO substrates with a flat surface, but having a different crystal structure owing to the lattice mismatch. The structure was determined to be a body-centred orthorhombic *Imma* with a unit cell of $a = 0.774$ nm and $b = c = 0.552$ nm. This strain-induced change of crystal structure is believed to contribute to the insulating property in the LCMO ultrathin films.

Acknowledgement

References

[1] R. Van Helmolt, J. Weckerg, B. Holzapfel, *et al.*, Phys. Rev. Lett. **71** 2331 (1993).
[2] S. Jin, T.H. Tiefel, M. McCormack, *et al.*, Science **264** 413 (1994).
[3] C.N.R. Rao and A.K. Cheetham, Science **272** 369 (1996).
[4] J.N. Eckstein, I. Bozovic, J. O'Donnell, *et al.*, Appl. Phys. Lett. **69** 1312 (1996).
[5] H.S. Wang, Q. Li, K. Liu, *et al.*, Appl. Phys. Lett. **74** 2212 (1999).
[6] J. O'Donnel, J.N. Eckstein and M.S. Rzchowski, Appl. Phys. Lett. **76** 218 (2000).
[7] Y. Suzuki, H.Y. Hwang, S.-W. Cheong, *et al.*, Appl. Phys. Lett. **71** 140 (1997).
[8] A.M. Haghiri-Gosnet, J. Wolfman, B. Merecy, *et al.*, J. Appl. Phys. **88** 4257 (2000).
[9] J. Dho, Y.N. Kim, Y.S. Hwang, *et al.*, Appl. Phys. Lett. **82** 1434 (2003).
[10] H.S. Wang, E. Wertz, Y.F. Hu, *et al.*, J. Appl. Phys. **87** 7409 (2000).
[11] J.Z. Sun, D.W. Abraham, R.A. Rao, *et al.*, Appl. Phys. Lett. **74** 3017 (1999).
[12] O.I. Lebedev, G. van Tendeloo, S. Amelinckx, *et al.*, Phys. Rev. B **58** 8065 (1998).
[13] H.W. Zandbergen, S. Freisem, T. Nojima, *et al.*, Phys. Rev. B **60** 10259 (1999).
[14] H.W. Zandbergen, J. Jansen, S. Freisem, *et al.*, Phil. Mag. A **80** 337 (2000).
[15] Z.Q. Yang, R. Hendrikx, J. Aarts, *et al.*, Phys. Rev. B **70** 174111 (2004).
[16] P.G. Radaelli, D.E. Cox, M. Marezio, *et al.*, Phys. Rev. Lett. **75** 4488 (1995).
[17] Q. Huang, A. Santoro, J.W. Lynn, *et al.*, Phys. Rev. B **58** 2684 (1998).
[18] H.W. Zandbergen and J. Jansen, Ultramicroscopy **80** 59 (1999).
[19] Y.H. Li, K.A. Thomas, P.S.I.P.N. de Silva, *et al.*, J. Mater. Res. **13** 2161 (1998).
[20] Z.Q. Yang, R. Hendrikx, J. Aarts, *et al.*, Phys. Rev. B **67** 024408 (2003).
[21] A. de Andrés, J. Rubio, G. Castro, *et al.*, Appl. Phys. Lett. **83** 713 (2003).
[22] A.M. Glazer, Acta Cryst. B **28** 3384 (1972).
[23] P.W. Woodward, Acta Cryst. B **53** 32 (1997).
[24] Th. Hahn (Editor), *International Tables for Crystallography*, Vol. A (Kluwer Academic Publishers, Dordrecht, 2002).